Green's theorem in time-reversal acoustics, back propagation and source-receiver redatuming

A tutorial

Wapenaar, K.; Brackenhoff, J.; Thorbecke, J.

DOI
10.3997/2214-4609.201900828

Publication date
2019

Document Version
Final published version

Published in
81st EAGE Conference and Exhibition 2019

2019 EAGE ANNUAL
81ST CONFERENCE + EXHIBITION
LONDON | THE UNITED KINGDOM

Tu_R04_05

Green's Theorem in Time-Reversal Acoustics, Back Propagation and Source-Receiver Redatuming: a Tutorial

K. Wapenaar[1]*, J. Brackenhoff[1], J. Thorbecke[1]

[1] Delft University of Technology

Summary

Time-reversal acoustics, seismic interferometry, back propagation, source-receiver redatuming and imaging by double focusing are all based in some way or another on Green's theorem. An implicit assumption for all these methods is that data are available on a closed boundary, a condition that is never met in geophysical practice. As a consequence, although direct and primary scattered waves are handled very well, most methods do not properly account for multiply scattered waves. This can be significantly improved by replacing the back-propagating Green's functions in any of the aforementioned approaches by Marchenko-based focusing functions. We show how this improves time-reversal acoustics, back propagation and source-receiver redatuming and we indicate how it enables the monitoring and forecasting of responses to induced seismic sources.

Introduction

Imaging methods for passive- and active-source data, such as time-reversal acoustics, seismic interferometry, back propagation, source-receiver redatuming and imaging by double focusing, can all be derived in a systematic way from Green's theorem. We review a selection of those methods, using the classical representation of the homogeneous Green's function as a starting point. A limitation is that this representation is expressed as a closed-boundary integral, which in practice can only be evaluated when the medium is accessible from all sides. We also discuss modifications of the imaging methods, based on a single-sided homogeneous Green's function representation, and show that these methods perform better than the classical methods when the medium is accessible from a single boundary (the earth's surface).

Representations of the homogeneous Green's function

The classical representation of the homogeneous Green's function reads in the space-frequency $(\mathbf{x},\omega)$ domain (Porter, 1970; Oristaglio, 1989)

$$G_{\mathrm{h}}(\mathbf{x}_B,\mathbf{x}_A,\omega) = \oint_{\mathbb{S}} \frac{1}{i\omega\rho(\mathbf{x})}\Big(\{\partial_i G(\mathbf{x},\mathbf{x}_B,\omega)\}G^*(\mathbf{x},\mathbf{x}_A,\omega) - G(\mathbf{x},\mathbf{x}_B,\omega)\partial_i G^*(\mathbf{x},\mathbf{x}_A,\omega)\Big)n_i \mathrm{d}\mathbf{x}. \quad (1)$$

Here $\mathbb{S}$ is an arbitrarily shaped closed boundary, with outward pointing normal vector $\mathbf{n} = (n_1,n_2,n_3)$, enclosing the points $\mathbf{x}_A$ and $\mathbf{x}_B$. $G(\mathbf{x},\mathbf{x}_A,\omega)$ is the Green's function and $G_{\mathrm{h}}(\mathbf{x}_B,\mathbf{x}_A,\omega) = G(\mathbf{x}_B,\mathbf{x}_A,\omega) + G^*(\mathbf{x}_B,\mathbf{x}_A,\omega)$ is the homogeneous Green's function. Furthermore, ρ is the mass density, i the imaginary unit and the asterisk denotes complex conjugation. When the medium outside $\mathbb{S}$ is homogeneous and $\mathbb{S}$ is sufficiently smooth, this representation may be approximated by

$$G_{\mathrm{h}}(\mathbf{x}_B,\mathbf{x}_A,\omega) = -2\oint_{\mathbb{S}} \frac{1}{i\omega\rho(\mathbf{x})}G(\mathbf{x},\mathbf{x}_B,\omega)\partial_i G^*(\mathbf{x},\mathbf{x}_A,\omega)n_i \mathrm{d}\mathbf{x}. \quad (2)$$

The complex-conjugated Green's function under the integral can be seen as a focusing function which focuses at $\mathbf{x}_A$, however, this only holds when it converges to $\mathbf{x}_A$ equally from all directions. This can be achieved by emitting it into the medium from a closed boundary $\mathbb{S}$. For practical situations we need another type of focusing function, which, when emitted into the medium from a single boundary $\mathbb{S}_0$, focuses at $\mathbf{x}_A$. Figure 1 illustrates the principle. In the single-sided homogeneous Green's function representation, the focusing function replaces the complex-conjugated Green's function, as follows

$$G_{\mathrm{h}}(\mathbf{x}_B,\mathbf{x}_A,\omega) = 4\Re\int_{\mathbb{S}_0} \frac{1}{i\omega\rho(\mathbf{x})}G(\mathbf{x},\mathbf{x}_B,\omega)\partial_3\big(f_1^+(\mathbf{x},\mathbf{x}_A,\omega) - \{f_1^-(\mathbf{x},\mathbf{x}_A,\omega)\}^*\big)\mathrm{d}\mathbf{x} \quad (3)$$

(Wapenaar et al., 2016; Van der Neut et al., 2017). The focusing function can be retrieved from reflection data at $\mathbb{S}_0$ using the Marchenko method. In the following we assume the focusing function is available.

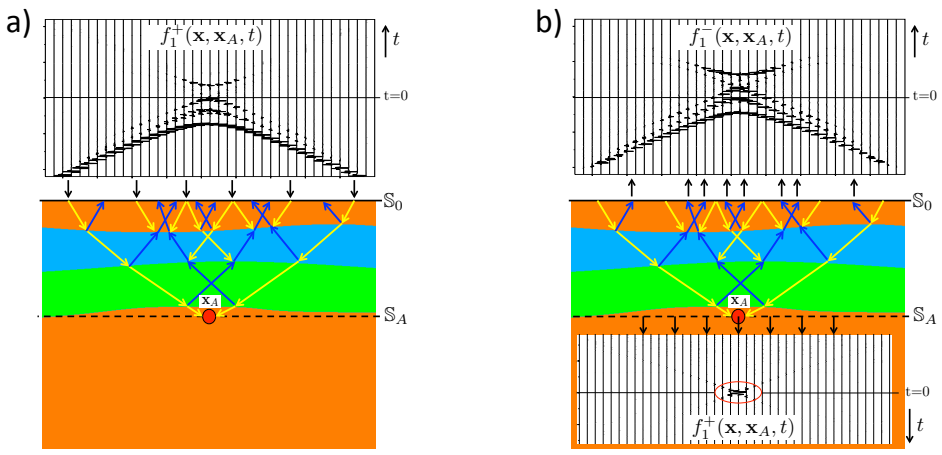

Figure 1 *The focusing function for the single-sided Green's function representation. (a) Emission of the downgoing focusing function from $\mathbb{S}_0$ into a truncated version of the actual medium. (b) Responses at $\mathbb{S}_0$ and $\mathbb{S}_A$.*

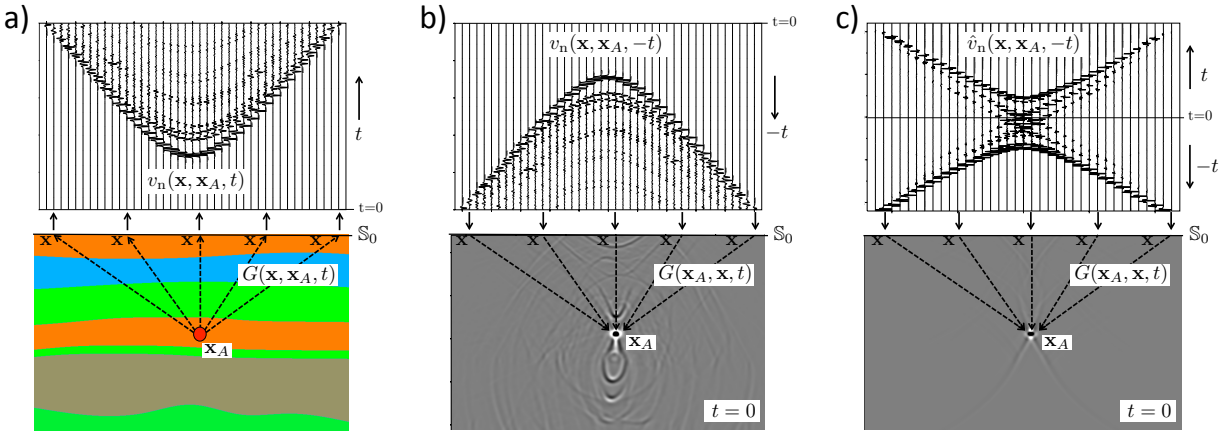

Figure 2 *Principle of time-reversal acoustics. (a) Forward propagation from $\mathbf{x}_A$ to the surface $\mathbb{S}_0$. (b) Emission of the time-reversed recordings $v_n(\mathbf{x},\mathbf{x}_A,-t)$ from $\mathbb{S}_0$ into the medium and snapshot of the wave field at $t=0$, with focus at $\mathbf{x}_A$. (c) Emission of a modified field $\hat{v}_n(\mathbf{x},\mathbf{x}_A,-t)$ into the medium. Note the improved focus.*

Time-reversal acoustics

The principle of time-reversal acoustics (Fink, 1992) is illustrated in Figure 2. Consider a source at $\mathbf{x}_A$ in the subsurface of which the response is recorded by receivers at $\mathbb{S}_0$ (Figure 2a). The recordings are denoted as $v_n(\mathbf{x},\mathbf{x}_A,t)$, where v_n stands for the normal component of the particle velocity. Using the equation of motion, we express v_n in the frequency domain as $v_n(\mathbf{x},\mathbf{x}_A,\omega)=\frac{1}{i\omega\rho(\mathbf{x})}n_i\partial_i G(\mathbf{x},\mathbf{x}_A,\omega)s(\omega)$, where $s(\omega)$ is the spectrum of the source at $\mathbf{x}_A$. Using this in the homogeneous Green's function representation of equation (2) we obtain $G_h(\mathbf{x}_B,\mathbf{x}_A,\omega)s^*(\omega)=2\oint_{\mathbb{S}}G(\mathbf{x}_B,\mathbf{x},\omega)v_n^*(\mathbf{x},\mathbf{x}_A,\omega)\mathrm{d}\mathbf{x}$, or, in the time domain,

$$G_h(\mathbf{x}_B,\mathbf{x}_A,t)*s(-t)=2\oint_{\mathbb{S}}\underbrace{G(\mathbf{x}_B,\mathbf{x},t)}_{\text{'propagator'}}*\underbrace{v_n(\mathbf{x},\mathbf{x}_A,-t)}_{\text{'source'}}\mathrm{d}\mathbf{x}, \tag{4}$$

where the inline asterisk ($*$) denotes temporal convolution. The right-hand side quantifies the emission of the time-reversed field $v_n(\mathbf{x},\mathbf{x}_A,-t)$ by sources at $\mathbf{x}$ on the boundary $\mathbb{S}$ (Figure 2b) and propagation of this field by the Green's function $G(\mathbf{x}_B,\mathbf{x},t)$ through the inhomogeneous medium to any point $\mathbf{x}_B$ inside $\mathbb{S}$; the integral is taken over all sources on $\mathbb{S}$ (Huygens' principle). The left-hand side quantifies the field at any point $\mathbf{x}_B$ inside $\mathbb{S}$. By setting $\mathbf{x}_B=\mathbf{x}_A$ and $t=0$ we obtain the field at the focus (Figure 2b). Note that in this example significant artefacts occur outside the focal position $\mathbf{x}_A$ because $\mathbb{S}_0$ is not a closed boundary. Next, we define a new particle velocity field, according to $\hat{v}_n^*(\mathbf{x},\mathbf{x}_A,\omega)=\frac{1}{i\omega\rho(\mathbf{x})}\partial_3\big(f_1^+(\mathbf{x},\mathbf{x}_A,\omega)-\{f_1^-(\mathbf{x},\mathbf{x}_A,\omega)\}^*\big)s(\omega)$, where for $s(\omega)$ we take a real-valued spectrum. Using this in equation (3) we obtain $G_h(\mathbf{x}_B,\mathbf{x}_A,\omega)s(\omega)=4\Re\int_{\mathbb{S}_0}G(\mathbf{x}_B,\mathbf{x},\omega)\hat{v}_n^*(\mathbf{x},\mathbf{x}_A,\omega)\mathrm{d}\mathbf{x}$, or, in the time domain,

$$G_h(\mathbf{x}_B,\mathbf{x}_A,t)*s(t)=2\int_{\mathbb{S}_0}G(\mathbf{x}_B,\mathbf{x},t)*\hat{v}_n(\mathbf{x},\mathbf{x}_A,-t)\mathrm{d}\mathbf{x}+2\int_{\mathbb{S}_0}G(\mathbf{x}_B,\mathbf{x},-t)*\hat{v}_n(\mathbf{x},\mathbf{x}_A,t)\mathrm{d}\mathbf{x}. \tag{5}$$

By setting again $\mathbf{x}_B=\mathbf{x}_A$ and $t=0$ we obtain the field at the focus (Figure 2c). Note that the artefacts have been significantly reduced. The remaining artefacts are due to the finite aperture and negligence of the evanescent field.

Back propagation

Given a wave field observed at the boundary of a medium, the field inside the medium can be obtained by back propagation. Figure 3a illustrates the principle. By interchanging $\mathbf{x}_A$ and $\mathbf{x}_B$ in equation (2) and multiplying both sides with a real-valued spectrum $s(\omega)$ of the source at $\mathbf{x}_A$, we obtain

$$p(\mathbf{x}_B,\mathbf{x}_A,\omega)+p^*(\mathbf{x}_B,\mathbf{x}_A,\omega)=\oint_{\mathbb{S}}F(\mathbf{x},\mathbf{x}_B,\omega)p(\mathbf{x},\mathbf{x}_A,\omega)\mathrm{d}\mathbf{x}. \tag{6}$$

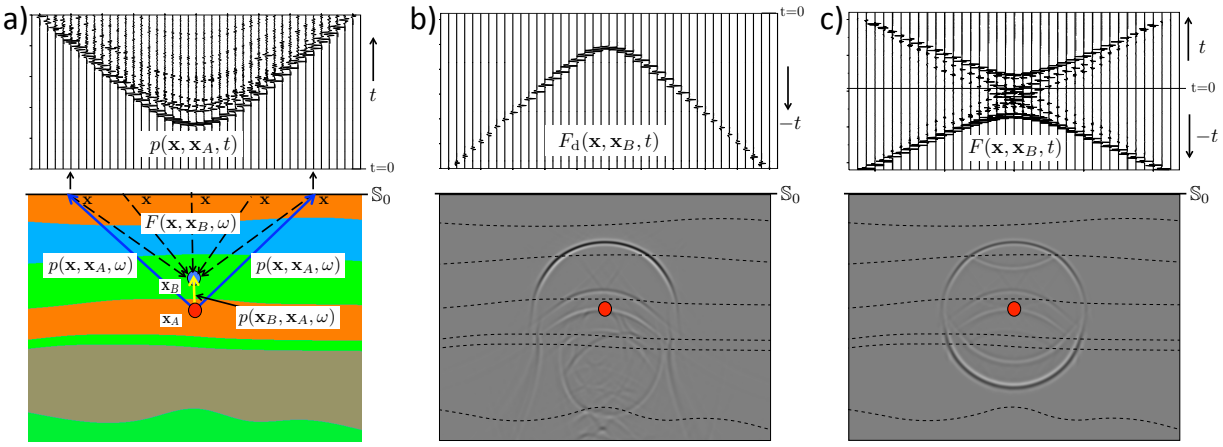

Figure 3 *Principle of back propagation. (a) The wave field $p(\mathbf{x},\mathbf{x}_A,t)$ at the boundary $\mathbb{S}_0$ and illustration of its back propagation to $\mathbf{x}_B$ inside the medium. (b) The back propagation operator $F_d(\mathbf{x},\mathbf{x}_B,t)$ and a snapshot of the back propagated wave field at $t_1 = 300$ ms for all $\mathbf{x}_B$. (c) Idem, for the improved back-propagation operator $F(\mathbf{x},\mathbf{x}_B,t)$. Note the improved snapshot.*

Here $p(\mathbf{x},\mathbf{x}_A,\omega) = G(\mathbf{x},\mathbf{x}_A,\omega)s(\omega)$ stands for the observed field at the boundary $\mathbb{S}$ and $F(\mathbf{x},\mathbf{x}_B,\omega) = -\frac{2}{i\omega\rho(\mathbf{x})}n_i\partial_i G^*(\mathbf{x},\mathbf{x}_B,\omega)$ for the back propagation operator, both in the frequency domain. Hence, in theory the exact field $p(\mathbf{x}_B,\mathbf{x}_A,\omega)$ can be obtained at any $\mathbf{x}_B$ inside the medium. Because in practical situations the field $p(\mathbf{x},\mathbf{x}_A,\omega)$ is observed only at a finite horizontal part $\mathbb{S}_0$ of the boundary, approximations arise in practise when $\mathbb{S}$ is replaced by $\mathbb{S}_0$. One of the consequences is that multiple reflections are not handled correctly. In practice the back propagation operator is often approximated by its direct contribution $F_d(\mathbf{x},\mathbf{x}_B,\omega) = \frac{2}{i\omega\rho(\mathbf{x})}\partial_3 G_d^*(\mathbf{x},\mathbf{x}_B,\omega)$. Figure 3b shows this back-propagation operator in the time domain and a snapshot of the back-propagated wave field. Note that the primary upgoing field is retrieved well, but parts of the field are missing and significant artefacts occur. Next, we derive in a similar way from equation (3)

$$p(\mathbf{x}_B,\mathbf{x}_A,\omega) + p^*(\mathbf{x}_B,\mathbf{x}_A,\omega) = 2\Re\int_{\mathbb{S}_0} F(\mathbf{x},\mathbf{x}_B,\omega)p(\mathbf{x},\mathbf{x}_A,\omega)\mathrm{d}\mathbf{x}, \tag{7}$$

with $F(\mathbf{x},\mathbf{x}_B,\omega) = \frac{2}{i\omega\rho(\mathbf{x})}\partial_3(f_1^+(\mathbf{x},\mathbf{x}_B,\omega) - \{f_1^-(\mathbf{x},\mathbf{x}_B,\omega)\}^*)$, see Figure 3c. Note that the snapshot shows the correctly retrieved wave field. This back propagation method has an interesting application in monitoring of induced seismicity. Assuming $p(\mathbf{x},\mathbf{x}_A,\omega)$ stands for the response to an induced seismic source at $\mathbf{x}_A$, this method creates, in a data-driven way, omnidirectional virtual receivers at any $\mathbf{x}_B$ to monitor the emitted field from the source to the surface. This application is discussed in a companion paper (Brackenhoff et al., 2019).

Source-receiver redatuming

In the previous section we discussed back propagation of data $p(\mathbf{x},\mathbf{x}_A,\omega)$, which is the response to a source at $\mathbf{x}_A$ inside the medium. Here we extend this process for the situation in which both the sources and receivers are located at the surface. First, in equation (7), we replace $\mathbb{S}_0$ by $\mathbb{S}_0'$ (just above $\mathbb{S}_0$), $\mathbf{x}$ by $\mathbf{x}' \in \mathbb{S}_0'$, $\mathbf{x}_A$ by $\mathbf{x} \in \mathbb{S}_0$ and $\mathbf{x}_B$ by $\mathbf{x}_A$. Next, we apply source-receiver reciprocity on both sides of the equation. This yields

$$p(\mathbf{x},\mathbf{x}_A,\omega) + p^*(\mathbf{x},\mathbf{x}_A,\omega) = 2\Re\int_{\mathbb{S}_0'} p(\mathbf{x},\mathbf{x}',\omega)F(\mathbf{x}',\mathbf{x}_A,\omega)\mathrm{d}\mathbf{x}', \tag{8}$$

with $F(\mathbf{x}',\mathbf{x}_A,\omega)$ defined similar as above. The field $p(\mathbf{x},\mathbf{x}',\omega) = G(\mathbf{x},\mathbf{x}',\omega)s(\omega)$ represents the data at the surface. Equation (8) back propagates the sources from $\mathbf{x}'$ on $\mathbb{S}_0'$ to $\mathbf{x}_A$. Source-receiver redatuming is now defined as the following two-step process. In step one, apply equation (8) to create an omnidirectional virtual source at any desired position $\mathbf{x}_A$ in the subsurface. According to the left-hand side, the response to this virtual source is observed by actual receivers at $\mathbf{x}$ at the surface. Isolate $p(\mathbf{x},\mathbf{x}_A,\omega)$ from the left-hand side by applying a time window (a simple Heaviside function) in the time domain. In

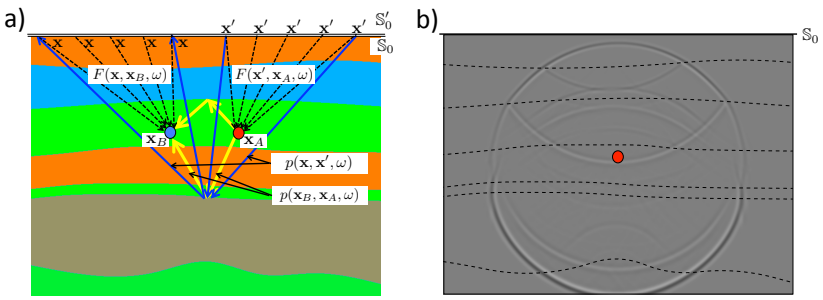

Figure 4 *(a) Principle of source-receiver redatuming. (b) Snapshot of the wave field* $p(\mathbf{x}_B,\mathbf{x}_A,t)$ *at* $t_2 = 500$ *ms.*

step two, substitute the retrieved response $p(\mathbf{x},\mathbf{x}_A,\omega)$ into equation (7) to create virtual receivers at any position $\mathbf{x}_B$ in the subsurface. Figure 4(a) illustrates the principle. Note the analogy with classical redatuming (Berryhill, 1984; Berkhout and Wapenaar, 1993) and source-receiver interferometry (Curtis and Halliday, 2010), except that their complex-conjugated Green's functions have been replaced by focusing operators. These operators can be obtained with the Marchenko method. Figure 4b shows a snapshot of $p(\mathbf{x}_B,\mathbf{x}_A,t)$. This method has an interesting application in forecasting the effects of induced seismicity. Assuming $\mathbf{x}_A$ is the position where induced seismicity is likely to take place, this method forecasts the response by creating, in a data-driven way, a virtual source at $\mathbf{x}_A$ and virtual receivers at any $\mathbf{x}_B$ that observe the propagation and scattering of its emitted field from the source to the surface. Also this method is further discussed in the companion paper (Brackenhoff et al., 2019). Another interesting application is imaging by double focusing (Staring et al., 2018).

Conclusions

The classical homogeneous Green's function representation, originally developed for optical image formation by holograms, expresses the Green's function plus its time-reversal between two arbitrary points in terms of an integral along a closed boundary enclosing these points. It forms a unified basis for a variety of seismic imaging methods, such as time-reversal acoustics, seismic interferometry, back propagation, source-receiver redatuming and imaging by double focusing. We have derived several of these methods by applying some simple manipulations to the classical homogeneous Green's function representation. However, in most cases multiple scattering is not correctly handled because in practical situations data are not available on a closed boundary. We also discussed a single-sided homogeneous Green's function representation, which requires access to the medium from one side only (the earth's surface). We used this single-sided representation as the basis for deriving modifications of time-reversal acoustics, back propagation and source-receiver redatuming. These methods do account for multiple scattering and can be used to obtain accurate images of the source or the subsurface, without artefacts related to multiple scattering. Another interesting application is the monitoring and forecasting of responses to induced seismic sources, which is discussed in a companion paper.

References

Berkhout, A.J. and Wapenaar, C.P.A. [1993] A unified approach to acoustical reflection imaging. Part II: The inverse problem. *J. Acoust. Soc. Am.*, **93**(4), 2017–2023.

Berryhill, J.R. [1984] Wave-equation datuming before stack. *Geophysics*, **49**, 2064–2066.

Brackenhoff, J., Thorbecke, J. and Wapenaar, K. [2019] Monitoring induced distributed double-couple sources using Marchenko-based virtual receivers. In: *EAGE, Extended Abstracts*.

Curtis, A. and Halliday, D. [2010] Source-receiver wavefield interferometry. *Phys. Rev. E*, **81**, 046601.

Fink, M. [1992] Time-reversal of ultrasonic fields: Basic principles. *IEEE T.U.F.F.C.*, **39**, 555–566.

Van der Neut, J., Johnson, J.L., van Wijk, K., Singh, S., Slob, E. and Wapenaar, K. [2017] A Marchenko equation for acoustic inverse source problems. *J. Acoust. Soc. Am.*, **141**(6), 4332–4346.

Oristaglio, M.L. [1989] An inverse scattering formula that uses all the data. *Inverse Problems*, **5**, 1097–1105.

Porter, R.P. [1970] Diffraction-limited, scalar image formation with holograms of arbitrary shape. *J. Opt. Soc. Am.*, **60**, 1051–1059.

Staring, M., Pereira, R., Douma, H., van der Neut, J. and Wapenaar, K. [2018] Source-receiver Marchenko redatuming on field data using an adaptive double-focusing method. *Geophysics*, **83**(6), S579–S590.

Wapenaar, K., Thorbecke, J. and van der Neut, J. [2016] A single-sided homogeneous Green's function representation for holographic imaging, inverse scattering, time-reversal acoustics and interferometric Green's function retrieval. *Geophys. J. Int.*, **205**, 531–535.